Inorganic Chemistry

ARTICLE

pubs.acs.org/IC

Group 6 Complexes with Iron and Zinc Heterometals: Understanding the Structural, Spectroscopic, and Electrochemical Properties of a Complete Series of M≡M···M′ Compounds

Michael Nippe,[†] Eckhard Bill,[‡] and John F. Berry*[,†]

[†]Department of Chemistry, University of Wisconsin—Madison, 1101 University Ave., Madison, Wisconsin 53706, United States

[‡]Max-Planck-Institut für Bioanorganische Chemie, Stiftstrasse 34-36 D-45470 Mülheim an der Ruhr, Germany

Supporting Information

ABSTRACT: Binuclear quadruply bonded complexes $Cr_2(dpa)_4$ (**1**, dpa = 2,2′-dipyridylamide), $Mo_2(dpa)_4$ (**2**), and $W_2(dpa)_4$ (**3**) react with anhydrous $FeCl_2$, yielding heterometallic compounds $CrCrFe(dpa)_4Cl_2$ (**4**), $MoMoFe(dpa)_4Cl_2$ (**5**), and $WWFe(dpa)_4Cl_2$ (**6**). These molecules are structurally similar, having a linear M≡M···Fe chain that is axially capped by chloride ions and is equatorially supported by the helically twisted dpa ligands. A structurally related zinc analog, $CrCrZn(dpa)_4Cl_2$ (**7**), can be prepared upon metalation of **1** with $ZnCl_2$. This reaction also persistently produces a 2:1 adduct of $ZnCl_2$ with **1**, $[Cr_2(dpa)_4](ZnCl_2)_2$ (**8**), which is in equilibrium with **7** and has the two zinc ions bound externally to the Cr_2 core and axial bridging chloro ligands attached to each Cr ion. The sole isolable product of the addition of $ZnCl_2$ to **3** is a 1:1 adduct, $[W_2(dpa)_4]ZnCl_2$ (**9**). The structurally related chain complexes **4**, **5**, **6**, and **7** are characterized by X-ray crystallography, UV−vis spectroscopy, cyclic voltammetry, and ^{57}Fe Mössbauer spectroscopy for the iron complexes in order to gain insights into the nature of heterometallic interactions, electronic excited states, and redox properties of these compounds, which have implications for all other M≡M···M′ molecules. Additionally, NMR spectroscopy has been used to gain insight into the mechanism of the metalation of **1** by Zn(II).

INTRODUCTION

Polynuclear heterometallic compounds have recently been of general interest for their unique electronic,[1] magnetic,[2] magnetoelectric,[3] structural,[4] reactivity,[5] and catalytic[6] properties. In addition, the perspective of understanding metal−metal interactions in small defined synthetic molecules may also offer insights applicable to biologically important heterometallic metallo-enzyme active sites.[7] We and others[8−12] have recently explored the use of binuclear metal−metal multiply bonded compounds as building blocks for new heterometallic systems. In particular, we have recently reported a variety of heterometallic M≡M···M′ frameworks that feature a diamagnetic quadruply bonded group 6 dimetal unit M≡M (M = Cr(II), Mo(II)) in proximity to a paramagnetic transition metal ion M′ (M′ = Mn(II),[13] Fe(II),[14] Co(II)[15]). Synthetic access to these molecules and systematic combinations of the metals M and M′ is achievable via a general synthetic route[9,14] in which a binuclear quadruply bonded precursor $M_2(dpa)_4$ (dpa =2,2′-dipyridylamide) is metalated by a divalent metal salt, furnishing $MMM'(dpa)_4Cl_2$.

Homotrimetallic molecules having the dpa equatorial ligand have been known for some time now,[1,16] and experiments to probe their electronic structures have been reported[17−20] and correlated with the results of electron transport measurements through the trimetallic chain.[21−23] It should be noted that the homometallic trichromium molecules,[24] and to some extent the tricobalt molecules,[25] have an unsymmetrical structure with one short and one long metal−metal separation, much like the heterometallic molecules discussed here. These heterometallic molecules bring up interesting new questions about electronic structure: what is the nature of the heterometallic interaction, and how does this interaction affect the redox and spectroscopic properties of the molecule? Unlike in the case of their homometallic analogs, where DFT methods have been somewhat successful,[18−20] the heterometallic molecules have defied computational methods. Thus, more experiments and more compounds are needed to address these questions.

Here, we present a series of M≡M···Fe complexes with M = Cr, Mo, or W and a new Cr≡Cr···Zn complex with which we can begin to answer these questions. The iron complexes are particularly attractive in that their electronic structure can be interrogated using ^{57}Fe Mössbauer spectroscopy, and the zinc compound enables us to probe the redox and spectroscopic properties of the Cr≡Cr unit in the presence of a metal that does not show redox behavior and is spectroscopically invisible. The results of investigation of these compounds allows us to make a general assessment of the electronic structures, redox, and spectroscopic properties of all M≡M···M′ compounds known to date.

The compounds discussed here are $Cr_2(dpa)_4$ (**1**), $Mo_2(dpa)_4$ (**2**), $W_2(dpa)_4$ (**3**), $CrCrFe(dpa)_4Cl_2$ (**4**), $MoMoFe(dpa)_4Cl_2$ (**5**), $WWFe(dpa)_4Cl_2$ (**6**), $CrCrZn(dpa)_4Cl_2$ (**7**), $[Cr_2(dpa)_4](ZnCl_2)_2$ (**8**), and $[W_2(dpa)_4]ZnCl_2$ (**9**). Compound **6** is the first of these linear heterotrimetallic molecules to be reported

Received: April 5, 2011
Published: July 14, 2011

that contains two third-row metals, and **7** is the first of these compounds that is diamagnetic, which has allowed us to observe its formation via ^{1}H NMR spectroscopy. Compounds **8** and **9** have Zn(II) ions bound externally to the dimetallic Cr_2 or W_2 core and appear to be intermediates in the formation of the linear chain compounds.

RESULTS AND DISCUSSION

Synthesis. The preparation of iron compounds **4**−**6** is achieved utilizing our earlier introduced synthetic protocol, in which the dinuclear quadruply bonded synthons $M_2(dpa)_4$ (M = Cr,[14] Mo,[15] W[26]) are metalated with anhydrous $FeCl_2$ (Scheme 1). The chromium/iron complex **4** can be synthesized in refluxing THF. However, due to the low solubility of $Mo_2(dpa)_4$ and $W_2(dpa)_4$ in common solvents and their stronger metal−ligand bonds, it is necessary to carry out the preparation of $MoMoFe(dpa)_4Cl_2$ (**5**) and $WWFe(dpa)_4Cl_2$ (**6**) in refluxing naphthalene at 220 °C. Removal of naphthalene, extraction with CH_2Cl_2, and subsequent crystallization from CH_2Cl_2/hexanes furnishes **5**·$2CH_2Cl_2$ and **6**·$2CH_2Cl_2$ in useful yields (43% and 59%, respectively).

Scheme 1

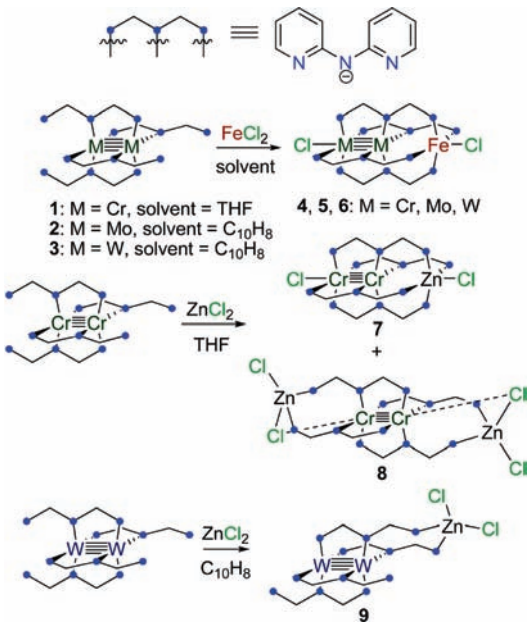

Preparation of heterometallic complexes containing zinc proved to be more challenging. Metalation of **1** was attempted using two methods. First, 1.3 equiv of $ZnCl_2$ in THF was used, in analogy to the reaction stoichiometry that has proved successful in preparing the Fe, Mn, and Co analogs.[13−15] Under these conditions, the brown product mixture contains the desired product, $CrCrZn(dpa)_4Cl_2$ (**7**), and a significant amount of the starting material (**1**). The presence of **1** in the product mixture is unusual in comparison to the results obtained for the high yielding metalation reactions of **1** with $MnCl_2$, $FeCl_2$, or $CoCl_2$ and indicates weaker and more reversible Zn^{2+} binding to the free pyridine moieties of the dpa ligands of **1**, likely due to weak and less selective metal−ligand interactions of the d^{10} Zn^{2+} ion. In an attempt to increase the yield of **7**, 4 equiv of $ZnCl_2$ was used in the reaction with **1**, which resulted in a rapid color change to green. In this case, a mixture of **7** and the red 2:1 Zn/Cr_2 adduct $[Cr_2(dpa)_4](ZnCl_2)_2$ (**8**) resulted. No reaction conditions were found for the selective, clean, quantitative formation of **7**, which is due to the inherent equilibrium nature of the system, as evidenced by ^{1}H NMR spectroscopy experiments (*vide infra*). Metalation of **3** with 3 equiv of $ZnCl_2$ was carried out in refluxing naphthalene, and this reaction afforded only one product, though it was not the anticipated linear chain compound. After workup, crystalline material of the very air-sensitive lilac 1:1 Zn/W_2 adduct $[W_2(dpa)_4]ZnCl_2$ (**9**) could be obtained from CH_2Cl_2/hexanes solvent mixtures, though the yield is poor, with the majority of the product being unreacted starting material.

Crystal Structures. Initially, **5** was crystallized from CH_2Cl_2/Et_2O mixtures, yielding monoclinic crystals of **5**·Et_2O ($P2_1/c$,

Table 1. Crystal Data

compound	**5**·$2CH_2Cl_2$, $Mo_2Fe(dpa)_4Cl_2$·$2CH_2Cl_2$	**5**·Et_2O, $Mo_2Fe(dpa)_4Cl_2$·Et_2O	**6**·$2CH_2Cl_2$, $W_2Fe(dpa)_4Cl_2$·$2CH_2Cl_2$	**7**·CH_2Cl_2, $Cr_2Zn(dpa)_4Cl_2$·CH_2Cl_2	**7**·Et_2O, $Cr_2Zn(dpa)_4Cl_2$·Et_2O	**8**·Et_2O·1.5THF, $Cr_2Zn_2(dpa)_4Cl_4$·Et_2O·1.5THF	**8**·hexanes, $Cr_2Zn_2(dpa)_4Cl_4$·hexanes
formula	$Mo_2FeC_{42}H_{36}N_{12}Cl_6$	$Mo_2FeC_{44}H_{42}N_{12}Cl_2O$	$W_2FeC_{42}H_{36}N_{12}Cl_6$	$Cr_2ZnC_{41}H_{34}N_{12}Cl_4$	$Cr_2ZnC_{44}H_{42}N_{12}Cl_2O$	$Cr_2Zn_2C_{46}H_{46}N_{12}Cl_4O_{1.5}$	$Cr_2Zn_2C_{46}H_{46}N_{12}Cl_4$
crystal system	monoclinic	monoclinic	monoclinic	orthorhombic	monoclinc	triclinic	triclinic
space group	$C2/c$	$P2_1/c$	$C2/c$	$Pnn2$	$P2_1/c$	$P\bar{1}$	$P\bar{1}$
a, Å	18.990(2)	16.200(3)	18.974(2)	12.8753(4)	15.9699(7)	12.6107(4)	12.6071(5)
b, Å	16.133(2)	15.749(3)	16.144(2)	14.0725(4)	15.7428(6)	15.2039(5)	15.2828(7)
c, Å	15.846(2)	17.034(3)	15.910(2)	11.3494(4)	17.0017(7)	16.3625(5)	16.3291(7)
α, deg	90	90	90	90	90	62.579(1)	116.321(2)
β, deg	112.345(1)	98.524(2)	112.823(1)	90	98.370(2)	70.665(2)	98.836(2)
γ, deg	90	90	90	90	90	78.582(2)	101.240(2)
V, Å^3	4490.3(8)	4298.1(13)	4491.6(7)	2056.4(1)	4228.8(3)	2623.8(1)	2660.8(2)
Z	4	4	4	2	4	2	2
ρ, Mg m^{-3}	1.730	1.659	1.989	1.625	1.563	1.523	1.320
R1,[a] $wR2$[b] ($I > 2\sigma(I)$)	0.0344, 0.0825	0.0271, 0.0670	0.0179, 0.0472	0.0252, 0.0652	0.0322, 0.0823	0.0307, 0.0813	0.0227, 0.0615
R1,[a] $wR2$[b] (all data)	0.0505, 0.0943	0.0333, 0.0718	0.0197, 0.0488	0.0257, 0.0654	0.0366, 0.0849	0.0345, 0.0831	0.0268, 0.0630

[a] $R1 = 3||F_o| - |F_c||/3|F_o|$. [b] $wR2 = [3[w(F_o^2 - F_c^2)^2]/3[w(F_o^2)^2]]^{1/2}$, $w = 1/\sigma^2(F_o^2) + (aP)^2 + bP$, where $P = [\max(0 \text{ or } F_o^2) + 2(F_c^2)]/3$.

dx.doi.org/10.1021/ic2011315 |*Inorg. Chem.* 2011, 50, 7650–7661

Table 2. Selected Bond Distances in 4,[14] 5, and 6

			5·Et_2O		
	4·CH_2Cl_2	5·$2CH_2Cl_2$	orientation 1 (69%)	orientation 2 (31%)	6·$2CH_2Cl_2$
Fe−Cl, Å	2.300(2)	2.337(1)	2.328(1)	2.375(3)	2.335(1)
Fe−N(avg), Å	2.157[4]	2.186[2]	2.204[3]	2.223[5]	2.191[9]
M···Fe, Å	2.715(2)	2.762(1)	2.648(2)	2.579(4)	2.718(1)
M≡M, Å	2.025(2)	2.104(1)	2.150(1)	2.210(4)	2.199(1)
M−N_a(avg), Å	2.028[2]	2.129[2]	2.124[2]	2.121[4]	2.106[2]
M−N_{py}(avg), Å	2.119[5]	2.214[2]	2.196[2]	2.172[3]	2.185[2]
M−Cl, Å	2.673(2)	2.747(1)	2.706(1)	2.667(2)	2.684(1)

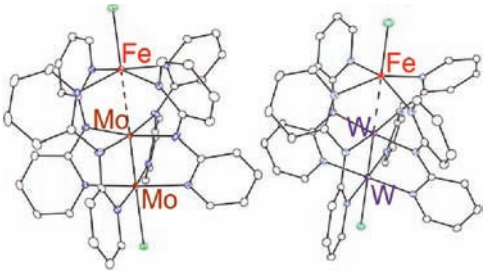

Figure 1. Molecular structures of **5** (left) and **6** (right) from **5**·$2CH_2Cl_2$ and **6**·$2CH_2Cl_2$ with displacement ellipsoids drawn at the 30% probability level. Hydrogen atoms have been omitted for clarity.

Table 1) in which the positions of the metal atoms are disordered such that the polar Mo≡Mo···Fe chain points in one of two opposing directions with relative occupancies of 0.69/0.31. The two crystallographically independent Fe ions have somewhat varying geometries (Table 2). Notably, there is no indication of disorder of the dpa moieties or the axial Cl ligands. However, crystallization of **5** and **6** from CH_2Cl_2/hexanes mixtures yields monoclinic crystals ($C2/c$) of **5**·$2CH_2Cl_2$ and **6**·$2CH_2Cl_2$ (Figure 1) in which no disorder of the metal atoms is present, and thus only one crystallographically independent Fe environment is observed. For the sake of simplicity, we will solely include the ordered CH_2Cl_2 solvates in the structural discussion and comparison with **4**·CH_2Cl_2.

The metal atoms and chloride ions in **5**·$2CH_2Cl_2$ and **6**·$2CH_2Cl_2$ occupy special positions along a crystallographic 2-fold rotator axis. The terminal metal atoms are equatorially ligated by four helically twisted dpa moieties and axially capped by Cl^- ions. The Mo≡Mo distance of 2.104(1) Å in **5** and the W≡W distance of 2.199(1) Å in **6** are within expectations for quadruple bonds of Mo and W.[27] The Mo≡Mo distance in **5** is almost identical to the that in **2** (2.097(2) Å), and the W≡W bond distance in **6** is also close to that in **3** (2.1934(4) Å).[26,28] One of the Mo or W atoms in **2** or **3**, respectively, is bound to central amide N-atoms (N_a) of the dpa ligand and the second is bound to pyridine N atoms (N_{py}). Both M−N_a (M = Cr, 2.028[2] Å; W, 2.106[2] Å; Mo, 2.129[2] Å) and M−N_{py} (M = Cr, 2.119[5] Å; W, 2.185[2] Å; Mo, 2.214[2] Å) distances increase in the order Cr < W < Mo. The M−N_a distances are shorter by as much as 0.08 Å than the M−N_{py} distances as a result of higher charge localization on N_a rather than N_{py} and stronger M−N_a bonds. We note that the inequality of M−N_a/M−N_{py} distances stands in stark contrast to the almost identical M−ligand bond lengths observed in the binuclear precursors $Cr_2(dpa)_4$ (2.05 Å/2.06 Å),[29] $Mo_2(dpa)_4$ (2.17 Å/2.18 Å),[28] and $W_2(dpa)_4$ (2.13 Å/2.13 Å).[26] It is thus apparent that the interaction between the M≡M unit and the equatorial dpa ligand is strongly affected by metalation, and a change in the charge distribution within the dpa ligand takes place, in which the strong M−N_a bonds dominate over the M−N_{py} and Fe−N_{py} interactions.

Most interestingly, substitution of Cr by Mo or W causes all Fe−ligand bonds to lengthen. The Fe−Cl distances in **5** and **6** are very similar at 2.337(1) Å and 2.335(1) Å, respectively, and are ∼0.03 Å longer than in **4**. Notably, these axial Fe−Cl bonds are not sensitive to the *trans* M···Fe separation, which is 0.04 Å shorter in **6** as compared to **5**. The equatorial Fe−N distances increase from 2.157[4] Å in **4** to 2.186[2] in **5** and 2.191[2] Å in **6**. This effect is ascribed to the longer M−N_a and M−N_{py} bonds, due to the increased ionic radii of Mo and W as compared to Cr, which causes increased space between the trimetallic chain and the dpa ligand, therefore increasing the Fe−N distances. Because of the increase in Fe−N bond lengths, the $[ClMo_2(dpa)_4]^-$ and $[ClW_2(dpa)_4]^-$ "ligands" are undoubtedly weaker donors to iron than is the $[ClCr_2(dpa)_4]^-$ species, but the Mo and W species are nevertheless strongly bound to the high-spin Fe(II) ion. In comparison to the crystal structures of other chloride-ligated high-spin Fe(II) complexes with pyridine donor ligands, the Fe−N distances in **5** and **6** are short. For example, in the simple octahedral complex *trans*-$FeCl_2$(pyridine)$_4$, the Fe−N bond distances are ∼2.23 Å,[30] longer than all of the Fe−N bond distances reported here, though this observation can be ascribed to the electron-donating amido nitrogen substituents available in the dpa ligand that are lacking in free pyridine. Ferrous complexes of other chelating pyridine donor ligands with alkyl donor substituents also show uniformly longer Fe−N bond distances >2.2 Å.[31,32]

Similar elongation of metal ligand bonds upon Cr≡Cr substitution by Mo≡Mo had been observed for Mn(II)[13] and Co(II)[15] analogs: The Mn−Cl and Mn−N distances are 0.07 Å and 0.05 Å longer in $MoMoMn(dpa)_4Cl_2$ than in $CrCrMn(dpa)_4Cl_2$. For the Co compounds $CrCrCo(dpa)_4Cl_2$ and $MoMoCo(dpa)_4Cl_2$, the variance in Co−ligand distances even causes a change in spin state, such that the Co ion in the former is mostly low-spin (S = 1/2) at 100 K, whereas the Co ion in the latter is high-spin (S = 3/2) down to very low temperatures.

Turning now to the zinc compounds, **7** (Figure 2, Table 3) crystallizes in the orthorhombic space group *Pnn*2 with a dichloromethane molecule of solvation, and this structure is isostructural with the earlier reported compounds $CrCrM(dpa)_4Cl_2\cdot CH_2Cl_2$ (M = Cr, Mn, Fe, Co).[13−15,24] The metal atoms are disordered over two orientations that are related by a

dx.doi.org/10.1021/ic2011315 |*Inorg. Chem.* 2011, 50, 7650–7661

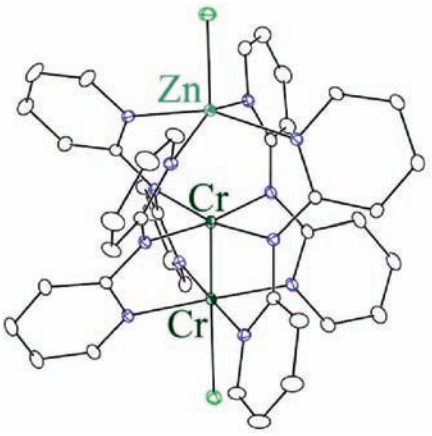

Figure 2. Molecular structure of **7** from **7**·CH_2Cl_2 with displacement ellipsoids drawn at the 30% probability level. Hydrogen atoms have been omitted for clarity.

Table 3. Bond Distances (Å) for Compound 7

		7·Et_2O	
	7·CH_2Cl_2	orientation 1 (56%)	orientation 2 (44%)
M−Cl, Å	2.2477(6)	2.2417(6)	2.2630(7)
M−N (avg), Å	2.160[2]	2.150[2]	2.156[2]
Cr···M, Å	2.780(2)	2.7700(8)	2.770(1)
Cr≡Cr, Å	1.997(2)	1.9916(9)	1.999(1)
Cr−N_a (avg), Å	2.026[2]	2.033[2]	2.031[2]
Cr−N_{py} (avg), Å	2.111[2]	2.116[2]	2.108[2]
Cr−Cl, Å	2.6904(7)	2.6617(1)	2.6319(1)

2-fold axis through the center of the molecule perpendicular to the trimetallic axis. In **7**·Et_2O ($P2_1/c$), the metal atoms of **7** are also similarly disordered, but two crystallographically independent and structurally very similar orientations with relative occupancies of 0.56/0.44 are present. The square-pyramidal Zn^{2+} ion in **7**·CH_2Cl_2 (**7**·Et_2O) is located 2.780(2) Å (2.770[1] Å) away from the Cr_2 unit and features Zn−N distances of 2.160[2] Å (2.153[1] Å) and a Zn−Cl distance of 2.2477(6) Å (2.252[1] Å). The other bond distances in **7** are very similar to those of the other Cr≡Cr···M compounds, and a general summary of the structural features within this series will be given later on in this paper.

Compound **8** (Figure 3, Table 4) was obtained in the form of the two triclinic (P) solvates **8**·1.5hexanes and **8**·Et_2O·1.5THF. The two crystallographically independent Zn^{2+} ions in **8**·1.5hexanes/**8**·Et_2O·1.5THF are four coordinate in a distorted tetrahedral geometry with averaged Zn−$Cl_{terminal}$, Zn−$Cl_{bridging}$, and Zn−N distances of 2.2317[3] Å/2.2323[5] Å, 2.2271[3] Å/2.2389[5] Å, and 2.029[1] Å/2.028[2] Å. The Zn···Cr distance is long (~3.23 Å) and the Cr≡Cr bond length of ~2.38 Å is much longer (~ 0.4 Å) than in **7** and **1**. In fact, it is one of the longest Cr≡Cr bonds in Cr dpa complexes, but similar to those observed in axially ligated tetrakis-carboxylate compounds (2.30[33]−2.41[34] Å) and the axially free tetrakis(2-phenylbenzoato)-dichromium compound (2.35 Å).[35] The unusually long Cr≡Cr distance is a result of weak coordination to the chloride ions of the $ZnCl_2$ groups. These bridging chloro ligands have a nearly right Zn−Cl···Cr angle of 82−83°, which maximizes the ability of the chloro ligand to donate electron

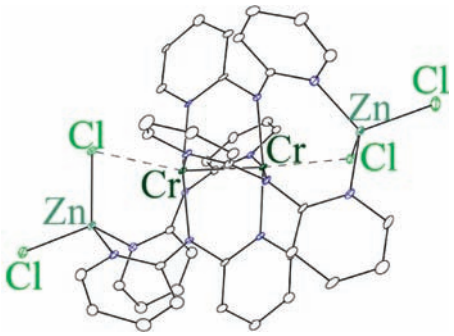

Figure 3. Molecular structure of **8** from **8**·Et_2O·1.5THF with displacement ellipsoids drawn at the 30% probability level. Hydrogen atoms have been omitted for clarity.

Table 4. Bond Lengths in 8·1.5hexanes and 8·Et_2O·1.5THF

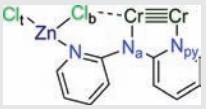

	8·1.5hexanes	**8**·Et_2O·1.5THF
Zn−Cl_t, Å	2.2317[3]	2.2323[5]
Zn−Cl_b, Å	2.2271[3]	2.2389[5]
Zn−N, Å	2.029[1]	2.028[2]
Cr−Cr, Å	2.3884(2)	2.3819(4)
Cr−N_a, Å	2.0833[9]	2.082[2]
Cr−N_{py}, Å	2.1227[9]	2.122[2]
Cr···Cl_b, Å	2.719[1]	2.726[1]

density to both metals using its valence p orbitals, though the Cl···Cr distance of ~2.72 Å is fairly long. Stronger coordination of chloride ions to a quadruply bonded Cr_2 center exists in the glycine complex $[Cr_2(O_2CCH_2NH_3)_4Cl_2]^{2+}$, which has Cr−Cl and Cr≡Cr bond distances of 2.58 and 2.52 Å, respectively.[36] Like in the other heterometallic structures, the amido Cr−N_a bond distances in **8** are shorter than the pyridine Cr−N_{py} bonds.

Despite numerous attempts with different crystallization conditions, only poor quality and severely disordered crystal structures of **9** (Figure S1, Supporting Information) could be obtained.[37] While the quality of the data precludes a detailed discussion of bond distances, an unambiguous structural assignment can be made. The $ZnCl_2$ unit in **9** is bound on the outside of the molecule by two pyridine donors that are twisted away from the W_2 center.

Mössbauer Spectroscopy. Although compounds **5** and **6** are structurally very similar, they are significantly different from **4** in that all of their iron-ligand bond lengths are longer than in the Cr analog. These structural changes may be ascribed to the larger radii of molybdenum and tungsten vs chromium, as discussed above, or one may invoke a direct heterometallic interaction to explain them. In order to differentiate between these two possibilities, a direct probe of the electronic structure of the iron center is useful. To this end, ^{57}Fe−Mössbauer spectroscopy experiments of crystalline samples of **5** and **6** (Figure 4, Table 5) were conducted to compare them to the earlier reported Mössbauer spectrum[13] of **4**. The key pieces of information that can be obtained from the Mössbauer spectra are the isomer shift

dx.doi.org/10.1021/ic2011315 |*Inorg. Chem.* 2011, 50, 7650–7661

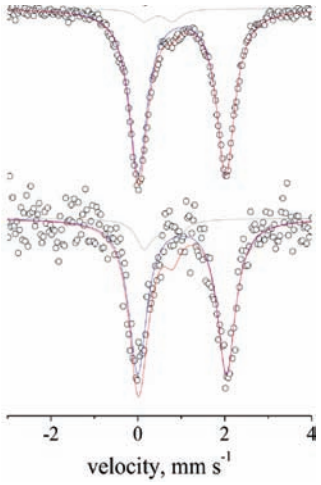

Figure 4. ^{57}Fe—Mössbauer spectra of **5** (top) and **6** (bottom) acquired at 80 K. The solid lines are simulations that include a small amount of ferric impurity.

Table 5. Mössbauer Parameters for Compounds 4,[13] 5, and 6 at 80 K

compound	δ, mm/s	ΔE_Q, mm/s	relative intensity, %
4·CH_2Cl_2	1.01	2.39	42.4
	1.01	1.63	57.6
5·$2CH_2Cl_2$	1.02	2.02	100
6·$2CH_2Cl_2$	1.02	2.04	100

(δ), which is sensitive to the iron oxidation state and coordination number, and the quadrupole splitting (ΔE_Q), which is a measure of the charge anisotropy of the iron, as manifested by an electric field gradient at the nucleus. The Mössbauer spectra of **5** and **6** each show one major signal with identical isomer shifts of 1.02 mm·s^{-1} and almost identical quadrupole splittings of 2.02 and 2.04 mm·s^{-1}, respectively. These values are indicative of a high-spin Fe(II)-containing compound, in good agreement with the observed iron—ligand bond distances of ~2.2 Å or greater in the crystal structures. The Mössbauer spectrum of **4** at this temperature features two signals of almost identical relative intensities, having the same δ of 1.01 mm s^{-1} but drastically different ΔE_Q values of 2.39 and 1.63 mm·s^{-1}. The two signals are due to the presence of two crystallographically distinct N_4FeCl geometries induced by a phase transition in **4**·CH_2Cl_2 at this temperature. This effect has recently been described in detail.[13] We can conclude from the ^{57}Fe—Mössbauer data analysis that the isomer shifts observed in **4**, **5**, and **6** are identical, signifying identical electron density at the Fe core in each compound; the ΔE_Q values in **5** and **6** are almost identical in agreement with the very similar N_4FeCl geometries.

It is remarkable that the δ values are insensitive to the increased iron—ligand bond distances in **5** and **6** as compared to **4** and are also insensitive to the different M···Fe distances in these compounds. The latter observation provides the most definitive evidence that little or no direct heterometallic bonding exists in these compounds. The former observation is harder to rationalize but is consistent with results of DFT calculations, where it was found that elongating an Fe—Cl bond by 0.15 Å had very little effect on the calculated value of δ, which only changed by ~0.03 mm s^{-1}.[13] The changes in iron—ligand bond distances between **4** and **5** and **6** are not nearly this extreme. It is possible that the changes in M···Fe and Fe—N distances offset each other in their contribution to δ, but there is currently no way to test this hypothesis.

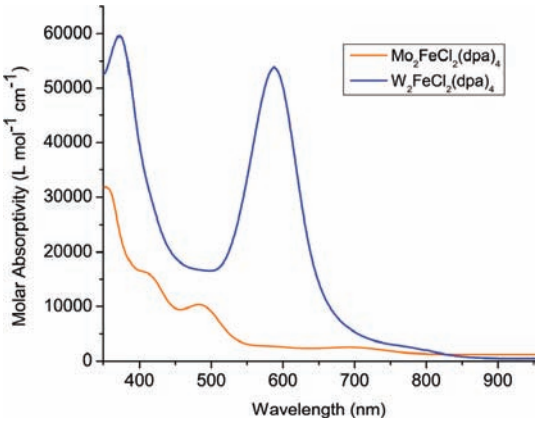

Figure 5. Electronic absorption spectra of **5** and **6**.

The similarity of the ΔE_Q values in **5** and **6** is also quite remarkable considering the large discrepancy in ΔE_Q for crystallographically inequivalent Fe sites in **4** that only differ due to crystal packing effects. The magnetic anisotropy of the M≡M quadruple bond has been proposed to make the ΔE_Q of the Fe centers in these compounds especially sensitive to the small geometric changes imposed by crystal packing forces.[13] One might therefore expect to see a more significant difference in the ΔE_Q values of **5** and **6**, since the diamagnetic anisotropies of Mo≡Mo and W≡W quadruple bonds have both been measured and found to be comparable to that for the Cr≡Cr bond,[27] but none is observed. This is because these compounds are exactly isostructural in their *C*2/*c* dichloromethane solvates (the form of the crystals used for Mössbauer measurements), and therefore the crystallographic environment of the Fe atoms in these compounds is exactly identical, leading to identical quadrupole splittings.

Electronic Absorption Spectroscopy. The heterotrimetallic chain complexes show rich absorption features in their visible spectra. Compound **4** has an absorption feature at 693 nm.[14] The absorption spectra of the Mo_2 and W_2 analogs **5** and **6** are shown in Figure 5. Charge transfer bands become more intense and lower in energy as the quadruply bonded unit is changed from Cr_2 to Mo_2 to W_2, as is expected for increased metal—ligand covalency and spin—orbit coupling. For the W_2 compound, in fact, an enormous charge transfer band at 588 nm is the most prominent feature of the spectrum. Lower intensity bands at lower energy, analogous to the 693 nm band in the CrCrFe complex, also appear in **5** and **6**. For **5**, an absorption at 693 nm is observed, which is shifted to 762 nm in **6**. These bands will be discussed further below. Additionally, there are bands at 1196 and 1047 nm in **5** and **6**, respectively, having very low intensity (molar absorptivities of 20 and 600 M^{-1} cm^{-1}, respectively), which are in the appropriate energy region to be classified as ligand field transitions centered at the distorted octahedral iron center.[38] It is rather remarkable that the Fe d—d bands in **5** and **6** are observable, since these have eluded detection in the chromium analogs. The increase in molar absorptivity by an order of magnitude from the MoMoFe complex to the WWFe complex

dx.doi.org/10.1021/ic2011315 |*Inorg. Chem.* 2011, 50, 7650–7661

Table 6. Data for the Complete Series of Cr≡Cr···M Compounds

compound	Cr≡Cr, Å	M···Cr_2, Å	M−N, Å	M−Cl, Å	λ_{max}, nm	$E_{1/2}$, V vs Fc/Fc^+	reference
$Cr_3(dpa)_4Cl_2$	2.241[3]	2.478[3]	2.117[2]	2.542[1]	673	∼−0.3[a]	24
$CrCrMn(dpa)_4Cl_2$	2.023[4]	2.807[4]	2.197[1]	2.256[1]	680		13
$CrCrFe(dpa)_4Cl_2$	2.029[2]	2.703[2]	2.153[2]	2.319[2]	693	−0.236	13, 14
$CrCrCo(dpa)_4Cl_2$ (high spin form)	2.067(5)	2.623(5)	2.125[3]	2.370(1)	696		15
$CrCrCo(dpa)_4Cl_2$ (low spin form)	2.036(5)	2.491(1)	2.054[2]	2.567(5)			15
$CrCrNi(dpa)_4Cl_2$	2.037(2)	2.585(2)	2.117[4]	2.360(2)			12
$CrCrZn(dpa)_4Cl_2$	1.996[1]	2.773[1]	2.155[2]	2.251[1]	687	−0.015	this work

[a] Approximation from original data given referenced to Ag/AgCl.

suggests that the Fe d−d bands gain intensity through spin−orbit coupling, and thus it is understandable that these bands have not been observed in the Cr complexes.

There are several possible assignments for the ∼700 nm bands in **4**, **5**, and **6**. One possible assignment is that these may be Fe d−d bands, companions to those transitions discussed above at ∼1100 nm that would be expected to appear in this energy region for a distorted octahedral iron complex. On the other hand, it is possible that the 700 nm bands are ligand field transitions within the metal−metal multiply bonded unit such as $\delta\rightarrow\delta^*$ transitions. Yet another possible assignment for this low energy transition is a metal-to-metal charge transfer (MMCT) band.

The Cr≡Cr···Zn complex **7** helps in the assignment of the electronic transitions in these compounds because the Zn^{2+} ion has no ligand-field transitions and is unable to undergo redox processes, rendering MMCT highly unlikely. Compound **7** does indeed have an absorption in the visible range at 687 nm, so this transition may be assigned to the Cr_2 quadruply bonded unit. Solomon and co-workers[39] assigned two sharp bands of extremely low intensity (ε = 1 M^{-1} cm^{-1}) at 624 and 616 nm in $Cr_2(OAc)_4(OH_2)_2$ as the Cr_2 triplet and singlet $\delta\rightarrow\delta^*$ transitions. The low intensity of these transitions, aside from the fact that the former is spin-forbidden, was ascribed to the weak δ overlap at a Cr≡Cr distance of ∼2.36 Å.[40] The band at 687 nm in **7** may therefore be tentatively assigned as the singlet Cr_2 $\delta\rightarrow\delta^*$ transition, which is more intense here than in $Cr_2(OAc)_4(OH_2)_2$ because of stronger δ overlap arising from the significantly shorter Cr≡Cr distance of ∼2.00 Å in **7**, as well as the lack of centrosymmetry in **7** as compared to $Cr_2(OAc)_4(OH_2)_2$. The lower energy of the $\delta\rightarrow\delta^*$ band in **7** vs $Cr_2(OAc)_4(OH_2)_2$ is most likely the result of the significant torsion angle of ∼22° in **7**, since twisting the δ bond is well-known to significantly impair orbital overlap,[41] even though the shorter metal−metal distance would be expected to increase the $\delta\rightarrow\delta^*$ energy.[42]

We note that features at almost the same energy are present in the electronic absorption spectra of $CrCrCr(dpa)_4Cl_2$ (674 nm),[24] **4** (693 nm),[14] $CrCrMn(dpa)_4Cl_2$ (680 nm), and $CrCrCo(dpa)_4Cl_2$ (696 nm) (see Table 6 and Figure S5, Supporting Information). These compounds all have similar Cr≡Cr bond distances close to 2 Å, with the exception of the trichromium molecule (2.24 Å), and similar torsion angles at the Cr_2 unit ranging from 21.5 to 22.4°, so it is reasonable to assume that the lowest energy absorptions in all of these compounds share a common origin. Though the assignment of these bands as Cr_2 $\delta\rightarrow\delta^*$ transitions is reasonable given the discussion above, the energies of these bands do not correlate with the Cr≡Cr bond distance, cos 2χ, with χ being the torsion angle around the Cr≡Cr bond, or the product of the two. Such a correlation would be expected for a true $\delta\rightarrow\delta^*$ transition. Instead, ignoring the outlier Cr_3 compound whose absorption spectrum is vastly different from those of the heterometallic compounds, the energies of these transitions track very closely the Cr_2···M heterometallic separations (Figure 6). This correlation suggests that, though this appears to be mainly a Cr_2 ligand field transition, this band also has some MMCT character. Whatever the origin of these transitions, it is likely that the bands at 693 and 762 nm in **5** and **6** arise from the same phenomenon.

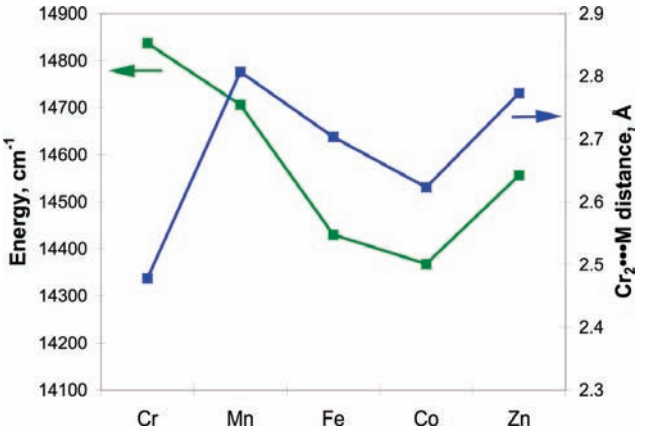

Figure 6. Correlation between the lowest energy absorption features and Cr_2···M heterometallic distances.

^{1}H NMR Study of the Metalation of 1. In addition to providing greater insight into the electronic spectra of heterometallic M≡M···M′ chains, the Zn(II) complex **7** gives us the opportunity to interrogate the mechanism by which these chain complexes form by using ^{1}H NMR spectroscopy. Analogous experiments with other metals have not been fruitful due to the paramagnetism of the first row transition metals involved. It should be noted that each metal atom in **1** is ligated by two amido N atoms (N_a) and two pyridine N atoms (N_{py}), leaving one pyridine moiety of the dpa ligand "dangling" on alternate sides of the M_2 unit. An interesting issue that we have not yet addressed in the conversion from **1** to the Cr≡Cr···M chains is the fact that metalation necessitates the breaking and forming of at least two M−N_a and two M−N_{py} bonds during rearrangement of the dpa ligands to furnish the general structural motif observed in the trinuclear products. Since different reaction temperatures are needed for the formation of Cr_2 chains (70 °C) vs Mo_2 or W_2 chains (220 °C), the energy required for this reaction certainly depends strongly on the strength of the M−ligand bonds.

The room temperature ^{1}H NMR spectrum of **1** in THF-d^8 displays eight signals of expected multiplicity and equal intensity

dx.doi.org/10.1021/ic2011315 |Inorg. Chem. 2011, 50, 7650–7661

Scheme 2

in the region from 5.8 to 8 ppm (Figure S2, Supporting Information). The spectrum thus indicates unsymmetrical binding of the four equivalent dpa ligands, which is in good agreement with the rough D_2 symmetry of the crystal structure. Furthermore, it indicates that the dpa ligand moieties do *not* scramble around the Cr≡Cr unit at this temperature. However, heating of **1** in THF-d^8 to 60 °C results in broadening of the individual multiplets, which suggests longitudinal shuffling of the dpa ligands at elevated temperatures.[43] In accord with the observations made on other dichromium complexes with dangling donor atoms,[43] the ligand shuffling is proposed to occur via the reaction pathway shown in Scheme 2 involving a symmetrical intermediate with a doubly chelating, bridging coordination mode of the dpa ligand. This particular coordination mode of the ligand is unusual but has been observed before in some binuclear compounds that have been crystallographically characterized.[26,44]

We have also investigated the ^{1}H NMR spectrum of **1** in the presence of 2 equiv of $ZnCl_2$ in THF at 0 °C (Figure S3, Supporting Information). The first spectrum, obtained 6 min after the addition of $ZnCl_2$ to **1**, shows no signals corresponding to **1**, indicating a rapid reaction of **1** with $ZnCl_2$ even at this low temperature. The spectrum features multiple broad signals in the region between 8.9 and 5.4 ppm that do not allow for any structural conclusions about the species present at this point of the reaction. We note, however, that the observed peak broadening is likely due to molecular fluxionality, in e.g. the reversible binding of Zn^{2+} or ligand shuffling as in Scheme 2. After 51 min at 0 °C, additional signals are observed at 9.28, 8.60, 7.19, 7.18, 6.73, 6.64, 6.48, and 6.45 ppm. These signals are less broad and better resolved and can clearly be assigned to **7**. Warming of the reaction mixture to room temperature increases the intensities of the signals corresponding to **7**. Thus, we are able to follow the formation of **7** from **1** by means of ^{1}H NMR and have observed a fluxional intermediate in this reaction.

Since **7** persistently cocrystallizes with **8**, we considered that **8** may be an intermediate in the formation of **7** and thus dissolved isolated red crystals of **8** in THF-d^8 at a low temperature (−10 °C). The corresponding ^{1}H NMR spectrum is shown in Figure S4 (bottom, Supporting Information). It displays broad features at 8.89, 8.55, 7.46, 6.79, 6.63, 6.04, and 5.79 ppm in addition to sharper signals of much smaller intensities. The broadness of the signals in the spectrum of **8** may be due to partial paramagnetic character of its very long Cr≡Cr bond (2.38 Å), in analogy to reported ^{1}H NMR studies of dichromium carboxylate and carbamate compounds, which have been shown to have very small, thermally accessible singlet $(\sigma^2\pi^4\delta^2)$−triplet $(\sigma^2\pi^4\delta\delta^*)$ separations of as little as 600 cm^{-1}.[45] However, the peak broadening may also indicate rapid ligand movement even at this low temperature, and it is a distinct possibility that the solution structure of **8** may not resemble its crystallographically determined solid state structure. Regardless of the exact assignment of this spectrum, the broad signals appear at similar chemical shifts to those observed for the intermediate species in the reaction of **1** with $ZnCl_2$ at 0 °C, which indicates the presence of the same species. The formulation of this species as

Scheme 3

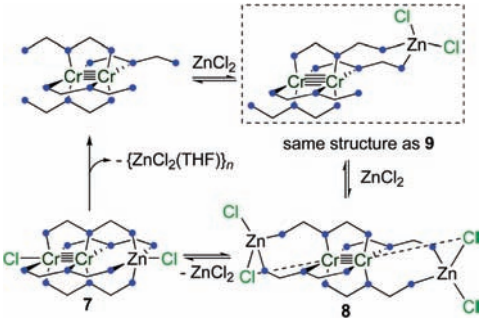

an intermediate during formation of **7** from **1** is further supported by the temperature dependence of the spectrum of **8**. Upon warming the solution to 25 °C, formation of **7** occurs in ∼8 min. Notably, **7** appears to be only metastable in THF solution, as we observe the formation of a white precipitate along with a color change of the solution to orange after 18 h at 25 °C. The ^{1}H NMR spectrum of this mixture (Figure S4, top, Supporting Information) shows signals corresponding to **1**. We propose that the demetalation of **7** to form **1** is prompted by the precipitation of a $ZnCl_2$ complex.

The results of the ^{1}H NMR studies may be combined as presented in Scheme 3. We propose that the conversion of **1** to **7** involves an initial 1:1 intermediate adduct having the same structural motif as **9**, even though it was not possible to isolate or observe this species. Since the ligand substitution kinetics for tungsten are much slower than they are for chromium, it is reasonable to assume that this intermediate may be trapped in the tungsten case and not observed in the chromium case. The addition of another equivalent of soluble $ZnCl_2$ yields the isolable intermediate **8**, which is in equilibrium with the trinuclear target compound **7**. Prolonged dissolution of **7** results in its demetalation to yield **1** and an insoluble $ZnCl_2$ species. We note that soluble $ZnCl_2$ is known to be present as the slightly distorted tetrahedral $ZnCl_2(THF)_2$ complex,[46] and a THF-insoluble form exists as a coordination polymer of formula $[ZnCl(C_4H_8O)(\mu\text{-}Cl)]_\infty$.[47] Thus, the addition of $ZnCl_2(THF)_2$ to **1** to form **8** is tantamount to the simple displacement of two THF ligands by pyridine moieties while retaining the tetrahedral molecular geometry around the Zn^{2+} ion. Such a simple ligand displacement mechanism is likely not feasible for other related MCl_2 salts which form isolable multinuclear $M_4Cl_8(THF)_6$ clusters in THF.[48] Thus, the generality of this mechanism to other first row MCl_2 species is not clear. It should be noted, however, that the mechanism proposed in Scheme 3 does account for our observations about the reaction conditions used to form **7**. When $ZnCl_2$ is provided in a roughly 1:1 stoichiometry, a mixture of **7** and **1** results because of the irreversible loss of the $ZnCl_2$ polymer, and when an excess of $ZnCl_2$ is provided, the equilibrium shifts to generate a mixture of **7** and **8**.

Electrochemistry. The heterotrimetallic molecules studied here are electrochemically active. We have performed an extensive investigation of the electrochemical properties of the quadruply bonded precursors **2** and **3** in order to aid in assigning the redox events in their heterometallic progeny.[26,49] Although **1** has been previously reported,[29] its electrochemical properties have not. While **2** and **3** both show reversible one-electron redox waves corresponding to the $M_2^{4+/5+}$ couple, oxidation of **1** is

dx.doi.org/10.1021/ic2011315 |*Inorg. Chem.* 2011, 50, 7650–7661

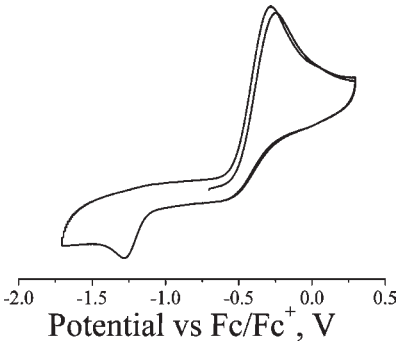

Figure 7. Cyclic voltammogram of **1** in CH_2Cl_2 solution with a glassy carbon working electrode, platinum wire auxiliary electrode, and Ag/Ag^+ reference electrode. Potentials are referenced to the ferrocene/ferrocenium couple that was measured by adding ferrocene to the solution.

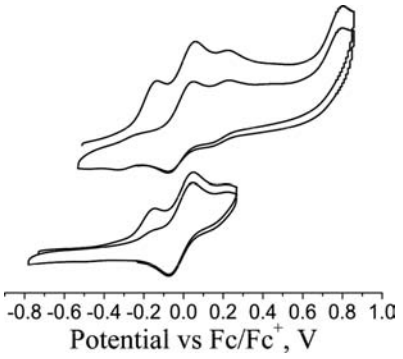

Figure 8. Cyclic voltammogram of **2** in CH_2Cl_2 at different scan ranges.

electrochemically irreversible, having a wave at $E_{ox} = -287$ mV in CH_2Cl_2 solution (Figure 7). This result is in accord with the commonly observed destruction of quadruply bonded Cr_2^{4+} compounds upon oxidation to yield mononuclear Cr^{3+} compounds.

Before we discuss the iron compounds, it is useful first to examine the effect of adding a nonredox active metal ion into the coordination sphere of the Cr_2 unit. The CV of **7** (Figure 8) features one major, quasi-reversible signal at $E_{1/2} = -15$ mV and one irreversible feature at 797 mV. Both features can unambiguously be assigned to oxidations of the Cr_2 unit within **7** due to the redox-inactivity of Zn^{2+}. This first oxidation occurs at ~300 mV higher potential than in **1**, consistent with the addition of a dicationic metal center in the coordination sphere of the Cr_2 unit. It is remarkable that rearrangement of the dpa ligands in going from **1** to **7** enables the Cr≡Cr unit to now show reversible oxidation behavior. The only other reported dichromium compound to display such properties is the tetrakis-guanidinate compound $Cr_2[(PhN)_2CN(CH_2)_4]_4$,[50] in which the $Cr_2^{4+/5+}$ redox couple occurs at a somewhat lower potential ($E_{1/2} = 0.02$ V vs Ag/AgCl in THF). Additionally, it was found that a small irreversible feature at −150 mV is present solely in the initial scan of the CV of **7**. The feature appears at higher potential than the oxidation of **1**, which suggests coordination of $ZnCl_2$ to $Cr_2(dpa)_4$, and we therefore assign this signal to the oxidation of another Cr_2/Zn complex, possibly of similar molecular structure to that of **8** or **9**.

As for the iron complexes, **4** has been reported to show a reversible one-electron wave at −236 mV (in CH_2Cl_2, referenced versus ferrocene/ferrocenium Fc/Fc^+) and an irreversible oxidation at 538 mV.[14] The former oxidation was assigned to the $Fe^{2+/3+}$ redox couple, based on the EPR signal of *in situ* generated $\mathbf{1}^+$. This assignment is bolstered by the data presented above for the zinc compound **7**, in which Cr_2 oxidation was found to occur at −15 mV. We would not expect that the replacement of a Zn^{2+} ion with an Fe^{2+} ion would change the oxidation potential of a Cr_2 unit by over 200 mV, so the −236 mV oxidation in **4** is soundly assigned as an $Fe^{2+/3+}$ couple.

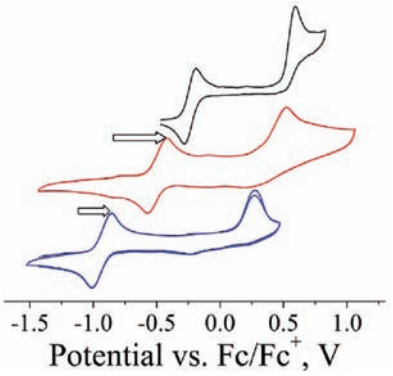

Figure 9. CVs of **4** (top),[14] **5** (middle), and **6** (bottom) in CH_2Cl_2 in 0.1 M NBu_4PF_6. Arrows indicate deviation of the potential of $M_2^{4+/5+}$ oxidation in $M_2Fe(dpa)_4Cl_2$ from $M_2(dpa)_4$ precursors.

The heterometallic Mo_2Fe and W_2Fe complexes have longer Fe−ligand bond distances than are observed for **4**. Thus, the Fe oxidation is expected to appear at a higher potential in compounds **5** and **6** due to the weaker ligand field at Fe. The CVs of **5** and **6** (Figure 9) both feature a reversible oxidation wave at very low potential ($E_{1/2}(\mathbf{5}) = -495$ mV; $E_{1/2}(\mathbf{6}) = -935$ mV) and one irreversible oxidation at higher potential ($E_{irrev.}(\mathbf{5}) = 412$ mV, $E_{irrev.}(\mathbf{6}) = 189$ mV). The first reversible oxidation for **5** and **6** can undoubtedly be assigned to the $M_2^{4+/5+}$ redox couple, which has been established to occur at −832 and −1193 mV in the binuclear precursors $Mo_2(dpa)_4$ and $W_2(dpa)_4$, respectively.[26] The rearrangement of the ligand and addition of $FeCl_2$ increases the stability of the M≡M unit toward oxidation by 337 and 258 mV for M = Mo and M = W, respectively, which is in accord with the 300 mV stabilization of the $Cr_2^{4+/5+}$ oxidation by Zn discussed above. The irreversible second oxidations of $\mathbf{5}^+$ and $\mathbf{6}^+$ at higher potentials result most likely in the decomposition of the analyte, presumably via loss of Fe(III). Thus, the CVs of **5** and **6** appear qualitatively similar to the CV of **4**, but the origin of the redox events in **5** and **6** occur at the M_2^{4+} unit in contrast to the ferrous to ferric transformation in **4**.

Overview of the Complete Cr≡Cr···M Series. At this point, the entire series of $CrCrM(dpa)_4Cl_2$ complexes with M = Cr−Zn has been reported, with the sole exception of the Cu(II) analog. From attempts made in our lab to generate the CrCrCu species, it appears that Cu(II) is too oxidizing to be incorporated into such a complex, as we have only been able to obtain Cu(I) byproducts.[51] Indeed, Peng and co-workers have reported a $\{RuRuCu\}^{6+}$ chain that is best described as having a Ru_2^{5+} unit connected to a Cu^+ ion.[11] It therefore seems appropriate to make a generalized comparison among the complexes of this series in light of the new results presented here on the MMFe and CrCrZn compounds. The pertinent data are collected together in Table 6, and it should be noted that all of the metals attached to the Cr_2 unit are high spin, such that the ground states are as

dx.doi.org/10.1021/ic2011315 |*Inorg. Chem.* 2011, 50, 7650–7661

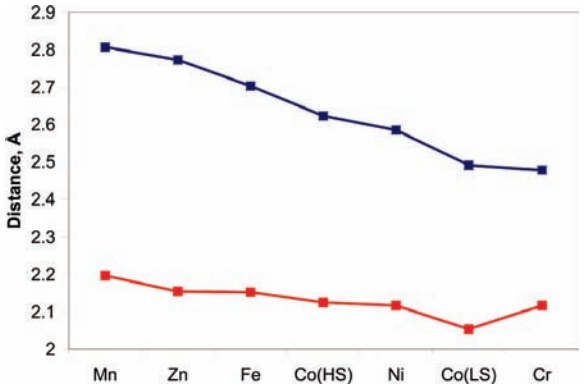

Figure 10. Correlated trend of the M···Cr_2 (blue) and M−N (red) bond distances across the series of CrCrM compounds.

follows: Cr $S = 2$, Mn $S = 5/2$, Fe $S = 2$, Co $S = 3/2$ (but at low temperatures a change to $S = 1/2$ takes place), Ni $S = 1$, and Zn $S = 0$.

The Cr≡Cr bond distances in this series of compounds span a remarkably narrow range, from 2.00 to 2.07 Å, with the notable exception of the homometallic trichromium compound. In general, the metal−metal distances in quadruply bonded Cr_2 complexes are extremely sensitive to axial donor ligands, so the insensitivity of these distances to the Mn−Zn "ligands" is an important indication that there is little sharing of electrons between the Cr and the heterometal centers. However, the Cr≡Cr distance of 2.24 Å in the homometallic analog along with the relatively close Cr···Cr distance of 2.48 Å suggest a σ delocalization in this molecule, as has been suggested from computational studies.[19] The view that there is little or no bonding interaction between the Cr≡Cr unit and the heterometals is further bolstered by a comparison of the heterometallic separations and the M−N bond distances (Figure 10). Both of these metal−"ligand" distances become smaller as the size of the metal decreases in the series from Mn > Zn > Fe > Co (high-spin) > Ni > Co (low-spin) > Cr. This series follows the expected trend in covalent radii for these elements with the exception of Cr as noted above.[52] The fact that the trends in M···Cr and M−N distances mirror each other shows that the M···Cr distances are governed solely by the size of M and not by electronic factors such as heterometallic bonding. Interestingly, the M−Cl bond distances do not follow this trend. One of the reasons for this is that the M−Cl bond distances can sometimes be significantly altered by crystal packing forces, which is an effect we have discussed in detail elsewhere.[13] The two longest M−Cl bond distances, 2.54 Å for Cr and 2.57 Å for Co (low spin), are best seen as the result of elongation due to Jahn−Teller distortion.

Analogous data on MoMoM and WWM complexes is limited, since only MoMoFe, MoMoMn,[13] and MoMoCo[15] species have been prepared, and the WWFe complex reported here is the first example of a WWM compound. Regardless, the available structural data follow the trend outlined above with the M···Mo(W) and M−N distances decreasing from M = Mn to Fe to Co, following the expected trend in effective nuclear charge.

CONCLUSIONS

Reported here are new heterometallic compounds of quadruply bonded group 6 dinuclear units in combination with iron or zinc. These compounds complete two distinct series, which provide insight into the nature of the heterometallic interactions in these compounds and how they affect the compounds' physical properties. The series of MMFe complexes with M = Cr, Mo, or W has been investigated using Mössbauer spectroscopy with the result that the isomer shift of the iron, a sensitive probe of oxidation states and coordination numbers, is insensitive to the identity of M. In the CrCrM series with M = Cr, Mn, Fe, Co, Ni, and Zn, the trend in Cr···M distances largely mirrors that of the M−N distances, indicating that these distances are largely determined by the size of M. These two results, taken together, are a strong indication that little or no heterometallic bonding occurs in these compounds. The CrCrZn complex also allows for an assignment of the electronic and redox properties of these compounds since it contains the redox inactive and spectroscopically invisible Zn(II) ion. The major feature at ∼700 nm in the absorption spectra of all CrCrM compounds is consistent with assignment as a $\delta \rightarrow \delta^*$ transition within the Cr_2 unit with some MMCT character. Analogous transitions appear in the Mo_2 and W_2 complexes, but these are dwarfed by charge transfer bands. Additionally, Fe ligand field transitions at ∼1100 nm have been observed for the first time in the MoMoFe and WWFe compounds. The $Cr_2^{4+/5+}$ redox couple in **7** occurs at −15 mV vs ferrocene/ferrocenium, which confirms the assignment of the first oxidation of **4** as an $Fe^{2+/3+}$ wave. First oxidations of **5** and **6** appear to be centered on the quadruply bonded Mo_2 or W_2 unit.

EXPERIMENTAL SECTION

Materials and Methods. All reactions were carried out under a dry N_2 atmosphere using Schlenk techniques and glovebox methods. Solvents diethyl ether (Et_2O), acetonitrile (CH_3CN), and hexanes were purified using a Vacuum Atmospheres solvent purification system. Dichloromethane was freshly distilled under a N_2 atmosphere over CaH_2 prior to use. Anhydrous $FeCl_2$ (Strem) was purchased and used as received. The ligand dpaH (2,2′-dipyridylamine, Sigma-Aldrich) was recrystallized from hot hexanes prior to use. $Cr_2(dpa)_4$,[14] CrCrFe-$(dpa)_4Cl_2$ (**1**),[14] $Mo_2(dpa)_4$,[26] and $W_2(dpa)_4$[26] were prepared according to literature procedures. Cyclic voltammograms (CVs) were taken on a BAS Epsilon-EC instrument using CH_2Cl_2 solutions with 0.1 M NBu_4PF_6 and <1 mM substrate. The electrodes were as follows: glassy carbon (working), Pt wire (auxiliary), and Ag/Ag^+ in CH_3CN (reference). The potentials were referenced versus the ferrocene/ferrocenium redox couple, by externally added ferrocene. Elemental analysis was carried out by Columbia Analytical Services in Arizona, United States. Mass spectrometry data were recorded at the Mass Spectrometry Facility of the Chemistry Instrument Center of the University of Wisconsin—Madison. Matrix-assisted laser desorption/ionization (MALDI) mass spectra were obtained using a Bruker REFLEX II spectrometer equipped with a 337 nm laser, a reflectron, delayed extraction, and a time-of-flight (TOF) analyzer. In the positive ion mode, the acceleration voltage was 25 kV. The IR spectra were taken on a BRUKER TENSOR 27 using KBr techniques. ^1H NMR spectra were recorded on a Varian INOVA-500 spectrometer. The reaction of **1** with 2 equiv of $ZnCl_2$ was monitored at ∼0 °C in proteo-THF, using a presaturation pulse to cancel out the THF signal at 3.58 ppm.

X-Ray Structure Determinations. Crystallographic data were measured at the Molecular Structure Laboratory of the Chemistry Department of the University of Wisconsin—Madison. Crystals were selected under oil under ambient conditions. Block shaped single crystals were attached to the tip of a MiTeGen MicroMount. The crystals were mounted in a stream of cold nitrogen at 100(1) K and centered in the X-ray beam using a video monitoring system. The crystal

evaluation and data collection were performed on a Bruker Quazar SMART APEX-II diffractometer with Mo Kα (λ = 0.71073 Å) radiation. The data were collected using a routine to survey the reciprocal space and were indexed by the SMART program.[53] The structures were solved using the Patterson method and refined by least-squares refinement on F^2 followed by difference Fourier synthesis.[54] All hydrogen atoms were included in the final structure factor calculation at idealized positions and were allowed to ride on the neighboring atoms with relative isotropic displacement coefficients.

The crystal structures **8**·1.5hexanes and **8**·Et_2O·1.5THF deserve additional comments. In **8**·1.5hexanes, there are ~1.5 hexanes solvent molecules present in the asymmetric unit. Attempts to model these entities using disorder models of hexanes with idealized geometries yielded unsatisfying results. Option SQUEEZE of the program PLATON[55] was used to correct the diffraction data and to identify the solvent molecule. The calculated upper limit of the volume that can be occupied by the solvent is 785 Å^3, or 29.5% of the unit cell volume. The program calculated 155 electrons in the unit cell for the diffuse species which corresponds to 1.5 hexanes molecules per $Cr_2Zn_2(dpa)_4Cl_4$ molecule (Z = 2). All derived results in the crystallographic tables are based on the known contents, and no data are given for the diffusely scattering species. In **8**·Et_2O·1.5THF, there is one THF and one Et_2O molecule well resolved per $Cr_2Zn_2(dpa)_4Cl_4$ molecule in the asymmetric unit. Additionally, it was found that Q peaks (Q1 = 2.2 e/Å^3) were present, which could not be accounted for and likely result from the partial presence of an additional solvent molecule. The calculated upper limit of the void volume is 169 Å^3, or 6.4% of the unit cell volume, containing 40 electrons in the unit cell for the diffuse species, corresponding to 0.5 THF molecules per $Cr_2Zn_2(dpa)_4Cl_4$ molecule (Z = 2). This THF electron density was handled analogously to the hexane molecule in **8**·1.5hexane.

MoMoFe(dpa)$_4$Cl$_2$ (5). A Schlenk flask containing a solid mixture of red $Mo_2(dpa)_4$ (300 mg, 0.34 mmol) and off-white $FeCl_2$ (70 mg, 0.55 mmol) in naphthalene (5 g) was placed into a preheated sand bath (~250 °C). The refluxing mixture was stirred for 30 min, after which a color change to brown was observed. The mixture was allowed to cool to room temperature and washed with hot hexanes (2 × 70 mL). Extraction with CH_2Cl_2 (30 mL) yielded a brown solution. Diffusion of either Et_2O or hexanes into the CH_2Cl_2 solution yielded crystals of **5**·Et_2O or **5**·2CH_2Cl_2, respectively. Yield: 170 mg, 43%. Anal. Calcd for $C_{44}H_{42}Cl_2Mo_2FeO_1N_{12}$ (**5**·Et_2O): C, 49.23%; H, 3.94%; N, 15.66%. Found: C, 49.66%; H, 3.39%; N, 15.58%. MALDI-TOF mass spectrum (amu): m/z 965 $[M - Cl]^+$, 872 $[M - FeCl_2]^+$. UV−vis (CH_2Cl_2 λ_{max}, nm (ε, M^{-1} cm^{-1})): 354 (30 000), 412 (20 000), 483 (10 000), 579 (sh, 3000), 693 (900), 1196 (20). IR (KBr, cm^{-1}): 1601 m, 1591 m, 1560 w, 1543 w, 1464 s, 1420 s, 1354 m, 1345 m, 1309 m, 1284 w, 1260 w, 1239 w, 1115 m, 1057 w, 1016 m, 1006 w, 883 w, 855 w, 768 m, 751 w, 740 m, 648 w, 635 w, 542 w, 518 w.

WWFe(dpa)$_4$Cl$_2$ (6). A Schlenk flask containing a solid mixture of dark purple $W_2(dpa)_4$ (210 mg, 0.20 mmol) and off-white $FeCl_2$ (70 mg, 0.55 mmol) in naphthalene (5 g) was placed into a preheated sand bath (~ 250 °C). The refluxing mixture was stirred for 1 h, after which a color change to blue was observed. The mixture was allowed to cool to room temperature and washed with hot hexanes (2 × 70 mL). Extraction with CH_2Cl_2 (30 mL) yielded a midnight blue solution. Diffusion of hexanes into the CH_2Cl_2 solution yielded crystals of **6**·2CH_2Cl_2. Yield: 160 mg, 59%. Anal. Calcd for $C_{40}H_{32}Cl_2W_2FeN_{12}$ (**3**): C, 40.88%; H, 2.74%; N, 14.30%. Found: C, 40.89%; H, 2.60%; N, 14.14%. MALDI-TOF mass spectrum (amu): m/z 1141 $[M - Cl]^+$, 1048 $[M - FeCl_2]^+$. UV−vis (CH_2Cl_2 λ_{max}, nm (ε, M^{-1} cm^{-1})): 370 (60 000), 588 (50 000), 762 (3000), 1047 (600). IR (KBr, cm^{-1}): 1599 m, 1588 m, 1560 w, 1472 m, 1462 s, 1415 s, 1338 m (br), 1307 m, 1283 w, 1257 w, 1235 w, 1153 m, 1057 w, 1018 w, 1005 w, 903 w, 858 w, 763 m, 738 m, 687 w, 636 w, 544 w, 517 w.

CrCrZn(dpa)$_4$Cl$_2$ (7) and Cr$_2$[(dpa)$_2$ZnCl$_2$]$_2$ (8). THF (35 mL) was added to a mixture of orange **1** (100 mg, 0.127 mmol) and white $ZnCl_2$ (70 mg, 0.511 mmol) while stirring, which caused an immediate color change to green-brown. The mixture was stirred for a minimum of 4 h at room temperature (25 °C) and subsequently worked up by one of the following procedures:

(a) The solvent was removed. The brown-green solid was extracted with CH_2Cl_2 (30 mL), and the brown-green solution was layered with hexanes. Yellow-green block-shaped crystals of **7**·CH_2Cl_2 grew within one day along with red needle-shaped crystals of **8**·1.5hexanes.

(b) Filtration of the THF solution and subsequent diffusion of Et_2O in the green-brown solution yielded block-shaped yellow-green crystals of **7**·Et_2O and red needle-shaped crystals of **8**·Et_2O·1.5THF. Due to the presence of both **7** and **8** in the product mixture, we cannot report accurate yields for either compound.

Each of these procedures yields substantial amounts of product, but the exact yields are strongly dependent on reaction conditions: time, temperature, and crystallization conditions. ^{1}H NMR data for **7** (THF-d^8, 500 MHz, ppm): δ 9.28 (4H, d), 8.60 (4H, d), 7.19 (4H, t), 7.18 (4H, t), 6.73 (4H, d), 6.64 (4H, d), 6.48 (4H, t), 6.45 (4H, t). Vis data for **7** in CH_2Cl_2 (λ_{max}, nm): 687.

W$_2$(dpa)$_2$Zn(dpa)$_2$Cl$_2$ (9). A Schlenk flask containing a solid mixture of blue $W_2(dpa)_4$ (250 mg, 0.238 mmol), white anhydrous $ZnCl_2$ (90 mg, 0.658 mmol), and naphthalene (4.5 g) was placed in a preheated (~ 250 °C) sand bath and stirred under mild reflux for 1 h, which caused a color change from dark blue to lilac. The mixture was allowed to cool to room temperature and was washed with hexanes (2 × 70 mL), and the residue was dried under vacuum conditions. Extraction of the solid with CH_2Cl_2 (35 mL) yielded a lilac solution that was carefully layered with hexanes, and large lilac block-shaped crystals of **9** grew within 1 day and could be isolated from a significant amount of blue-purple precipitate. Yield: 40 mg; 13%. Anal. Calcd. for $C_{40}H_{32}Cl_2N_{12}W_2Zn$ (**9**): C, 40.55%; H, 2.72%; N, 14.19%. Found: C, 40.51%; H, 2.83%; N, 13.29%. The lower than expected N percentage is likely due to formation of intractable nitrides during combustion analysis. Similar results are obtained regardless of whether V_2O_5 oxidant is used in the analysis. IR (KBr, cm^{-1}): 1603 (s), 1565 (w), 1466 (s), 1429 (s), 1355 (m), 1301 (m), 1234 (m), 1153 (m), 1115 (w), 1056 (w), 1018 (m), 992 (w), 953 (w), 910 (w), 867 (m), 768 (s), 736 (m), 646 (w), 535 (w), 510 (w), 418 (w).

■ ASSOCIATED CONTENT

Supporting Information. Figures S1−S5 and crystallographic data in CIF format. This material is available free of charge via the Internet at http://pubs.acs.org.

■ AUTHOR INFORMATION

Corresponding Author
*E-mail: berry@chem.wisc.edu.

■ ACKNOWLEDGMENT

We thank the National Science Foundation for financial support under CHE-0745500. We thank Dr. Emily H. P. Tan and Dr. Charles G. Fry for helpful comments and support related to the ^{1}H NMR experiments and Eugenia Turov for providing the UV−vis data for **5** and **6**.

■ REFERENCES

(1) Berry, J. F. *Struct. Bonding (Berlin)*; Mingos, D. M. P., Parkin, G., Eds.; Springer-Verlag: Berlin, 2010; Vol. 136.

(2) (a) Harris, T. D.; Coulon, C.; Clérac, R.; Long, J. R. *J. Am. Chem. Soc.* **2011**, *133*, 123. (b) Liao, Y.; Shum, W. W.; Miller, J. S. *J. Am. Chem. Soc.* **2002**, *124*, 9336. (c) Verdaguer, M.; Girolami, G. S. In *Magnetism Molecules to Materials V*; Springer-Verlag: Berlin, 2005; pp 283.

(3) Navulla, A.; Tsirlin, A. A.; Abakumov, A. M.; Shpanchenko, R. V.; Zhang, H.; Dikarev, E. V. *J. Am. Chem. Soc.* **2011**, *133*, 692.

(4) Stavila, V.; Thurston, J. H.; Whitmire, K. H. *Inorg. Chem.* **2009**, *48*, 6945.

(5) (a) Diaconescu, P. L. *Acc. Chem. Res.* **2010**, *43*, 1352. (b) Thomas, C. M.; Napoline, J. W.; Rowe, G. T.; Foxman, B. M. *Chem. Commun.* **2010**, *46*, 5790.

(6) (a) Shafir, A.; Arnold, J. *Organometallics* **2003**, *22*, 567. (b) Mandal, S. K.; Roesky, H. W. *Acc. Chem. Res.* **2010**, *43*, 248. (c) Hildebrandt, A.; Wetzold, N.; Ecorchard, P.; Walfort, B.; Ruffer, T.; Lang, H. *Eur. J. Inorg. Chem.* **2010**, 3615. (d) Nikiforov, G. B.; Roesky, H. W.; Jones, P. G.; Oswald, R. B.; Noltemeyer, M. *Dalton Trans.* **2007**, 4149. (e) Belokon, Y. N.; Clegg, W.; Harrington, R. W.; Young, C.; North, M. *Tetrahedron* **2007**, *63*, 5287. (f) Kawthekar, R. B.; Ahn, C. H.; Kim, G. J. *Catal. Lett.* **2007**, *115*, 62. (g) Zhou, W.; Napoline, J. W.; Thomas, C. M. *Eur. J. Inorg. Chem.* **2011**, 2029.

(7) (a) Groysman, S.; Holm, R. H. *Biochemistry* **2009**, *48*, 2310. (b) Kim, E.; Chufan, E. E.; Kamaraj, K.; Karlin, K. D. *Chem. Rev.* **2004**, *104*, 1077. (c) Lee, S. C.; Holm, R. H. *Chem. Rev.* **2004**, *104*, 1135. (d) Holm, R. H.; Kennepohl, P.; Solomon, E. I. *Chem. Rev.* **1996**, *96*, 2239.

(8) (a) Pal, K.; Nakao, K.; Mashima, K. *Eur. J. Inorg. Chem.* **2010**, 5668. (b) Mashima, K. *Bull. Chem. Soc. Jpn.* **2010**, *83*, 299. (c) Mashima, K.; Shima, A.; Nakao, K.; Fukumoto, A.; Kaneda, Y.; Kusurni, Y. *Inorg. Chem.* **2009**, *48*, 1879. (d) Mashima, K.; Shimoyama, Y.; Kusumi, Y.; Fukumoto, A.; Yamagata, T.; Ohashi, M. *Eur. J. Inorg. Chem.* **2007**, 235.

(9) Ohashi, M.; Shima, A.; Ruffer, T.; Mizomoto, H.; Kaneda, Y.; Mashima, K. *Inorg. Chem.* **2007**, *46*, 6702.

(10) Liu, I. P. C.; Chen, C. H.; Chen, C. F.; Lee, G. H.; Peng, S. M. *Chem. Commun.* **2009**, 577.

(11) Huang, G. C.; Benard, M.; Rohmer, M. M.; Li, L. A.; Chiu, M. J.; Yeh, C. Y.; Lee, G. H.; Peng, S. M. *Eur. J. Inorg. Chem.* **2008**, 1767.

(12) Aydin-Canturk, D.; Nuss, H. *Z. Anorg. Allg. Chem.* **2011**, *637*, 543.

(13) Nippe, M.; Wang, J.; Bill, E.; Hope, H.; Dalal, N. S.; Berry, J. F. *J. Am. Chem. Soc.* **2010**, *132*, 14261.

(14) Nippe, M.; Berry, J. F. *J. Am. Chem. Soc.* **2007**, *129*, 12684.

(15) Nippe, M.; Victor, E.; Berry, J. F. *Eur. J. Inorg. Chem.* **2008**, 5569.

(16) (a) Berry, J. F. In *Multiple Bonds Between Metal Atoms*, 3rd ed.; Cotton, F. A., Murillo, C. A., Walton, R. A., Eds.; Springer Science and Business Media, Inc.: New York, 2005; pp 669. (b) Yeh, C. Y.; Wang, C.-C.; Chen, C. H.; Peng, S.-M. In *Redox Systems under Nano-Space Control*; Hirao, T., Ed.; Springer: Berlin, 2006.

(17) (a) Berry, J. F.; Cotton, F. A.; Daniels, L. M.; Murillo, C. A.; Wang, X. P. *Inorg. Chem.* **2003**, *42*, 2418. (b) Berry, J. F.; Cotton, F. A.; Lu, T. B.; Murillo, C. A.; Roberts, B. K.; Wang, X. P. *J. Am. Chem. Soc.* **2004**, *126*, 7082.

(18) (a) Lopez, X.; Benard, M.; Rohmer, M. M. *THEOCHEM* **2006**, *777*, 53. (b) Benard, M.; Berry, J. F.; Cotton, F. A.; Gaudin, C.; Lopez, X.; Murillo, C. A.; Rohmer, M. M. *Inorg. Chem.* **2006**, *45*, 3932. (c) Rohmer, M. M.; Benard, M. *J. Cluster Sci.* **2002**, *13*, 333. (d) Rohmer, M. M.; Strich, A.; Benard, M.; Malrieu, J. P. *J. Am. Chem. Soc.* **2001**, *123*, 9126.

(19) Benbellat, N.; Rohmer, M. M.; Benard, M. *Chem. Commun.* **2001**, 2368.

(20) (a) Pantazis, D. A.; Murillo, C. A.; McGrady, J. E. *Dalton Trans.* **2008**, 608. (b) Pantazis, D. A.; McGrady, J. E. *J. Am. Chem. Soc.* **2006**, *128*, 4128.

(21) Chae, D. H.; Berry, J. F.; Jung, S.; Cotton, F. A.; Murillo, C. A.; Yao, Z. *Nano Lett.* **2006**, *6*, 165.

(22) (a) Tsai, T. W.; Huang, Q. R.; Peng, S. M.; Jin, B. Y. *J. Phys. Chem. C* **2010**, *114*, 3641. (b) Shih, K. N.; Huang, M. J.; Lu, H. C.; Fu, M. D.; Kuo, C. K.; Huang, G. C.; Lee, G. H.; Chen, C. H.; Peng, S. M. *Chem. Commun.* **2010**, *46*, 1338. (c) Chen, I. W. P.; Fu, M. D.; Tseng, W. H.; Yu, J. Y.; Wu, S. H.; Ku, C. J.; Chen, C. H.; Peng, S. M. *Angew. Chem., Int. Ed.* **2006**, *45*, 5814. (d) Lin, S. Y.; Chen, I. W. P.; Chen, C. H.; Hsieh, M. H.; Yeh, C. Y.; Lin, T. W.; Chen, Y. H.; Peng, S. M. *J. Phys. Chem. B* **2004**, *108*, 959.

(23) Georgiev, V. P.; McGrady, J. E. *Inorg. Chem.* **2010**, *49*, 5591.

(24) Berry, J. F.; Cotton, F. A.; Lu, T.; Murillo, C. A.; Roberts, B. K.; Wang, X. *J. Am. Chem. Soc.* **2004**, *126*, 7082.

(25) Clerac, R.; Cotton, F. A.; Daniels, L. M.; Dunbar, K. R.; Kirschbaum, K.; Murillo, C. A.; Pinkerton, A. A.; Schultz, A. J.; Wang, X. P. *J. Am. Chem. Soc.* **2000**, *122*, 6226.

(26) Nippe, M.; Victor, E.; Berry, J. F. *Inorg. Chem.* **2009**, *48*, 11889.

(27) Cotton, F. A., *Multiple Bonds between Metal Atoms*, 3rd ed.; Springer Science and Business Media, Inc: New York, 2005.

(28) Suen, M. C.; Wu, Y. Y.; Chen, J. D.; Keng, T. C.; Wang, J. C. *Inorg. Chim. Acta* **1999**, *288*, 82.

(29) (a) Edema, J. J. H.; Gambarotta, S.; Meetsma, A.; Spek, A. L.; Smeets, W. J. J.; Chiang, M. Y. *J. Chem. Soc., Dalton Trans.* **1993**, 789. (b) Cotton, F. A.; Daniels, L. M.; Murillo, C. A.; Pascual, I.; Zhou, H. C. *J. Am. Chem. Soc.* **1999**, *121*, 6856.

(30) Long, G. J.; Clarke, P. J. *Inorg. Chem.* **1978**, *17*, 1394.

(31) (a) Gebbink, R.; Jonas, R. T.; Goldsmith, C. R.; Stack, T. D. P. *Inorg. Chem.* **2002**, *41*, 4633. (b) Goldsmith, C. R.; Jonas, R. T.; Cole, A. P.; Stack, T. D. P. *Inorg. Chem.* **2002**, *41*, 4642. (c) Wong, E. L. M.; Fang, G. S.; Che, C. M.; Zhu, N. Y. *Chem. Commun.* **2005**, 4578.

(32) (a) Quesada, M.; de Hoog, P.; Gamez, P.; Roubeau, O.; Aromi, G.; Donnadieu, B.; Massera, C.; Lutz, M.; Spek, A. L.; Reedijk, J. *Eur. J. Inorg. Chem.* **2006**, 1353. (b) Neville, S. M.; Leita, B. A.; Offermann, D. A.; Duriska, M. B.; Moubaraki, B.; Chapman, K. W.; Halder, G. J.; Murray, K. S. *Eur. J. Inorg. Chem.* **2007**, 1073.

(33) Cotton, F. A.; Rice, G. W. *Inorg. Chem.* **1978**, *17*, 2004.

(34) Cotton, F. A.; Extine, M. W.; Rice, G. W. *Inorg. Chem.* **1978**, *17*, 176.

(35) Cotton, F. A.; Thompson, J. L. *Inorg. Chem.* **1981**, *20*, 1292.

(36) Ardon, M.; Bino, A.; Cohen, S.; Felthouse, T. R. *Inorg. Chem.* **1984**, *23*, 3450.

(37) Compound **9** crystallized as $\mathbf{9}\cdot 1.28CH_2Cl_2$ in the monoclinic space group $P2_1/c$ with unit cell dimensions a = 12.1587(3) Å, b = 16.6233(5), c = 25.1776(8), and β = 100.771(2)° (cell voulme = 4999.2(3) Å; Z = 4). Least-square refinement yielded R1 and wR2 values of 0.0805 and 0.1981 for $I > 2\sigma(I)$ data and 0.0958 and 0.2086 for all data.

(38) Solomon, E. I.; Brunold, T. C.; Davis, M. I.; Kemsley, J. N.; Lee, S. K.; Lehnert, N.; Neese, F.; Skulan, A. J.; Yang, Y. S.; Zhou, J. *Chem. Rev.* **2000**, *100*, 235.

(39) Rice, S. F.; Wilson, R. B.; Solomon, E. I. *Inorg. Chem.* **1980**, *19*, 3425.

(40) Cotton, F. A.; DeBoer, B. G.; LaPrade, M. D.; Pipal, J. R.; Ucko, D. A. *Acta Crystallogr., Sect. B* **1971**, *27*, 1664.

(41) Cotton, F. A.; Nocera, D. G. *Acc. Chem. Res.* **2000**, *33*, 483.

(42) Ferrante, F.; Gagliardi, L.; Bursten, B. E.; Sattelberger, A. P. *Inorg. Chem.* **2005**, *44*, 8476.

(43) Clérac, R.; Cotton, F. A.; Jeffery, S. P.; Murillo, C. A.; Wang, X. *Dalton Trans.* **2003**, 3022.

(44) (a) Berry, J. F.; Cotton, F. A.; Murillo, C. A. *Inorg. Chim. Acta* **2004**, *357*, 3847. (b) Cotton, F. A.; Daniels, L. M.; Murillo, C. A.; Zhou, H. C. *Inorg. Chim. Acta* **2000**, *305*, 69. (c) Muller-Buschbaum, K.; Quitmann, C. C. *Inorg. Chem.* **2006**, *45*, 2678.

(45) Cotton, F. A.; Chen, H.; Daniels, L. M.; Feng, X. *J. Am. Chem. Soc.* **1992**, *114*, 8980.

(46) Dashti, A.; Niediek, K.; Werner, B.; Neumüller, B. *Z. Anorg. Allg. Chem.* **2004**, *623*, 394.

(47) Bottomley, F.; Ferris, E. C.; White, P. S. *Acta Crystallogr., Sect. C* **1989**, *C45*, 816.

(48) (a) Cotton, F. A.; Luck, R. L.; Son, K.-A. *Inorg. Chim. Acta* **1991**, *179*, 11. (b) Zhao, H.; Clérac, R.; Sun, J.-S.; Ouyang, X.; Clemente-Juan, J. M.; Gómez-García, C. J.; Coronado, E.; Dunbar, K. R. *J. Solid State Chem.* **2001**, *159*, 281.

(49) Nippe, M.; Goodman, S. M.; Fry, C. G.; Berry, J. F. *J. Am. Chem. Soc.* **2011**, *133*, 2856.
(50) (a) Cotton, F. A.; Dalal, N. S.; Hillard, E. A.; Huang, P.; Murillo, C. A.; Ramsey, C. M. *Inorg. Chem.* **2003**, *42*, 1388. (b) Cotton, F. A.; Daniels, L. M.; Huang, P.; Murillo, C. A. *Inorg. Chem.* **2002**, *41*, 317.
(51) Nippe, M.; Berry, J. F. Unpublished results.
(52) Pyykko, P.; Atsumi, M. *Chem.—Eur. J.* **2009**, *15*, 186.
(53) *SMART*; Bruker-AXS: Madison, WI, 2009.
(54) Dolomanov, O. V.; Bourhis, L. J.; Gildea, R. J.; Howard, J. A. K.; Puschmann, H. *J. Appl. Crystallogr.* **2009**, *42*, 339.
(55) Spek, A. L. *J. Appl. Crystallogr.* **2003**, *36*, 7.